Active Learning for Data-Efficient Optimization of Entangled Granular Metamaterials

Peng Wang Gaoyan Shi Yu Guo**

Peng Wang, Yu Guo
Department of Engineering Mechanics, Zhejiang University, Hangzhou 310027, China
Email Address: 12224048@zju.edu.cn (P. Wang), yguo@zju.edu.cn (Y. Guo)

Gaoyan Shi
College of Design and Architecture, Zhejiang University of Technology, Hangzhou 310023, China

Yu Guo
State Key Laboratory of Clean Energy Utilization, Zhejiang University, Hangzhou 310027, China

Keywords: *Entangled granular matamaterials, optimal design, active learning, yield strength*

Entangled granular metamaterials derive exceptional macroscopic rigidity from the topological interlocking of their constituents yet rationally designing particle geometries that maximize this effect remains a formidable challenge due to the immense configuration space and the prohibitive computational cost of discrete element simulations. Here we present a data-efficient and uncertainty-aware design framework that enables the autonomous discovery of exceptional particle geometries to substantially enhance macroscopic yield strength beyond the reach of conventional heuristic shape families. This is achieved by integrating a Semi-Supervised Graph Wasserstein Autoencoder to embed discrete particle topologies into a continuous latent manifold while utilizing Langevin-based stochastic optimization to explore the structure-property landscape. By explicitly penalizing epistemic uncertainty through a Lower Confidence Bound acquisition strategy the framework robustly navigates the stochastic response landscape and avoids spurious optima under conditions of severe data scarcity. The discovered low-aspect-ratio particle geometries leverage cooperative geometric interlocking to impart quasi-cohesive behavior which results in yield strengths and self-supporting capabilities typically restricted to high-aspect-ratio slender fibers. Confined compression and angle-of-repose experiments on 3D-printed assemblies confirm high simulation fidelity and validate the emergence of geometry-driven load-bearing architectures in physical realizations. This work establishes a scalable paradigm for the autonomous discovery of complex architected materials and provides a powerful blueprint for the engineering of programmable matter through purely morphological control.

1 Introduction

Entangled granular metamaterials (EGMs), composed of non-convex macroscopic particles, constitute a unique class of disordered mechanical metamaterials widely used in applications ranging from impact-resistant shielding to reconfigurable civil infrastructure and soft robotics.[1–5] Unlike traditional assemblies of spherical grains that rely on weak frictional contacts,[6,7] EGMs derive an iconic macroscopic rigidity from the topological interlocking of their constituents.[8] In this regime, the mechanical integrity of the system is no longer solely governed by material properties but is dictated by the non-convex geometry of the individual grains. Through cooperative geometric interlocking, these complex shapes impart the material with exceptional yield strength and emergent self-supporting capabilities which effectively challenge the boundaries of classical granular physics.[9,10]

At present, the design of EGMs relies heavily on a discrete set of heuristic primitives such as U-shaped, Z-shaped, or hexapod particles.[9–14] Merely optimizing aspect ratios or limb angles within these fixed parametric families, however, fails to access the radical, free-form geometries required for maximizing mechanical interlocking. The macroscopic yield strength serves as a direct quantitative fingerprint of the microscopic topological interlocking capability where a higher yield strength signifies a more intricate network of geometric constraints that inhibit particle reorganization. By optimizing the particle geometry while keeping the constituent material constant, one can effectively treat the granular assembly as a programmable metamaterial. This paradigm offers an expansive design space for software-defined tuning

of mechanical properties solely through morphological engineering, thereby bypassing the need for complex chemical synthesis. However, a fundamental barrier remains the complete absence of universal design rules or predictive physical laws that can map arbitrary non-convex particle topologies to emergent macroscopic mechanical responses. As a result, no a priori principle exists to indicate which geometric motifs will yield superior performance, rendering human intuition largely ineffective in this regime. This challenge is further exacerbated by the curse of dimensionality and the prohibitive computational cost of high-fidelity discrete element method simulations, which together make iterative trial-and-error design strategies computationally intractable.[15–17]

To overcome these shortcomings, data-driven machine learning (ML) has emerged as an alternative working principle for the inverse design of architected metamaterials.[18–22] Deep generative models such as Variational Autoencoders (VAEs) offer the capacity to map high-dimensional geometric features onto continuous latent manifolds.[23,24] However, extending these paradigms to entangled granular media is non-trivial. The efficacy of such data-hungry models is typically predicated on the availability of massive labeled datasets which remains a critical bottleneck in granular mechanics where data acquisition is computationally expensive. Recently, Physics-Informed Machine Learning (PIML) has been proposed to improve data efficiency by leveraging partial differential equation (PDE) residuals.[25–27] Yet, transplanting such physics-embedding paradigms to entangled granular media presents a fundamental theoretical barrier. Unlike continuum systems governed by smooth PDEs, granular mechanics is driven by non-smooth, discrete contact dynamics. Lacking a closed-form governing equation to serve as a differentiable loss function, the design process remains restricted to a critically small-sample regime.

Moreover, the macroscopic mechanical response of a granular assembly is intrinsically stochastic and follows a probability distribution rather than a fixed scalar value.[28] Deterministic optimization approaches often overlook this inherent uncertainty by treating isolated simulation results as absolute ground truths. This approach risks the exploitation of statistical outliers or model hallucinations that fail to maintain robustness in physical reality. Therefore, a probabilistic framework is essential to robustly distinguish between genuinely superior geometries and artifacts arising from packing stochasticity.[29]

Here, we introduce a data-efficient and uncertainty-aware framework that embeds discrete particle topologies into a continuous latent space to enable reliable exploration and optimization of geometry-induced yield strength in entangled granular metamaterials. This framework integrates a Semi-Supervised Graph Wasserstein Autoencoder (SS-GWAE) with Langevin dynamics-based stochastic optimization. Our approach effectively embeds discrete particle topologies into a continuous and differentiable latent manifold which enables gradient-based navigation of the topological design space. To overcome the computational burden, we employ a semi-supervised strategy that leverages a massive corpus of unlabeled shapes to learn the intrinsic geometric manifold while anchoring the latent space to physical properties using only a sparse set of labeled simulations. Guided by a Lower Confidence Bound (LCB) acquisition function, the framework explicitly penalizes epistemic uncertainty to ensure the discovery of physically robust geometries. Finally, we bridge the gap between computational design and physical reality through additive manufacturing. Confined compression and Angle of Repose (AoR) tests on 3D-printed assemblies confirm that the optimized geometries exhibit emergent geometric cohesion to achieve self-supporting capabilities typically reserved for slender fibers.[30] These experiments demonstrate that geometry alone can endow disordered granular assemblies with effective cohesion and load-bearing capacity while establishing a scalable paradigm for the autonomous discovery of complex architected materials under strict data constraints.

2 Results and discussion

2.1 Geometry-Driven Mechanical Heterogeneity in Entangled Granular Metamaterials

Morphological exploration of entangled granular metamaterials is grounded in a rigorous geometric parameterization that connects simple heuristic primitives to a broad spectrum of non-convex geometries (**Figure 1a**). A linear rod with an aspect ratio of 7 ($AR = 7$) is selected as the geometric baseline, as this value marks the critical transition from friction-dominated packings to mechanically entangled, strain-hardening assemblies.[31] The baseline rod is discretized into an articulated chain of $N = 7$ spherical nodes with equal diameter, thereby preserving constant material volume and skeletal length while enabling substantial configurational flexibility.

The systematic parameterization of particle geometries is achieved by recursively defining the spatial configuration through a sequence of bond angles θ_i and dihedral angles φ_i as illustrated in Figure 1b. Let $\mathcal{P} = \{\mathbf{p}_0, \mathbf{p}_1, \ldots, \mathbf{p}_{N-1}\}$ denote the centers of the spherical nodes connected by fixed length bonds l_b. While the first two nodes $(\mathbf{p}_0, \mathbf{p}_1)$ establish the global orientation, the position of each subsequent node $\mathbf{p}_i$ is determined by a local spherical mapping relative to the preceding segments. At each step i where $i \geq 3$, a local orthonormal basis $\mathcal{F}_i = \{\mathbf{u}_i, \mathbf{v}_i, \mathbf{w}_i\}$ is anchored at $\mathbf{p}_{i-1}$ based on the history of the chain as defined in the equation.

$$\mathbf{u}_i = \frac{\mathbf{p}_{i-1} - \mathbf{p}_{i-2}}{\|\mathbf{p}_{i-1} - \mathbf{p}_{i-2}\|}, \quad \mathbf{w}_i = \frac{\mathbf{u}_i \times (\mathbf{p}_{i-3} - \mathbf{p}_{i-2})}{\|\mathbf{u}_i \times (\mathbf{p}_{i-3} - \mathbf{p}_{i-2})\|}, \quad \mathbf{v}_i = \mathbf{u}_i \times \mathbf{w}_i \tag{1}$$

This discrete frame defines a rotation matrix $\mathbf{R}_i = [\mathbf{u}_i, \mathbf{v}_i, \mathbf{w}_i]$ that characterizes the local orientation. The global coordinates of the i-th node are then updated through the recursive relation presented in

$$\mathbf{p}_i = \mathbf{p}_{i-1} + l_b \mathbf{R}_i \mathbf{d}(\theta_i, \varphi_i) \tag{2}$$

In this expression, the local displacement vector $\mathbf{d}(\theta_i, \varphi_i)$ is given in spherical coordinates by

$$\mathbf{d}(\theta_i, \varphi_i) = [\sin\varphi_i \cos\theta_i, \sin\varphi_i \sin\theta_i, \cos\varphi_i]^T \tag{3}$$

This formulation establishes a high-dimensional configuration space governed by five pairs of angular parameters that allows the baseline rod to be reconfigured into a broad spectrum of morphologies. These architectures range from planar primitives such as U-shaped and Z-shaped particles to fully three-dimensional chiral architectures as shown in Figure 1a. Importantly, this discretization strategy guarantees that any observed mechanical enhancement arises solely from morphological organization rather than changes in mass or aspect ratio.

A bonded-sphere-cylinder model[31] is employed to represent the complex non-convex geometries of individual grains within a Discrete Element Method (DEM) framework (Section S1, Supporting Information). Using this high-fidelity representation, we generated an initial dataset $\mathcal{D}_0$ of 240 distinct particle geometries through Latin Hypercube Sampling to ensure an unbiased coverage of the configuration space. The mechanical performance of each morphology-specific packing structure was characterized by triaxial compression simulations as illustrated in Figure 1c, d. Each granular assembly consisting of 2,000 identical particles was consolidated under a constant confining pressure of $\tau_c = 10$ kPa and subjected to vertical compression at a constant strain rate until an axial strain of 0.25 was reached. We extracted the macroscopic yield strength τ^*_{max} as the peak value of the normalized deviatoric stress $(\tau_y - \tau_c)/\tau_c$ where this metric serves as a quantitative indicator of the microscopic entanglement density. A higher τ^*_{max} signifies a more intricate network of geometric constraints that effectively inhibit particle reorganization and sliding. Consequently, maximizing τ^*_{max} through morphological engineering constitutes the primary objective of our autonomous design framework.

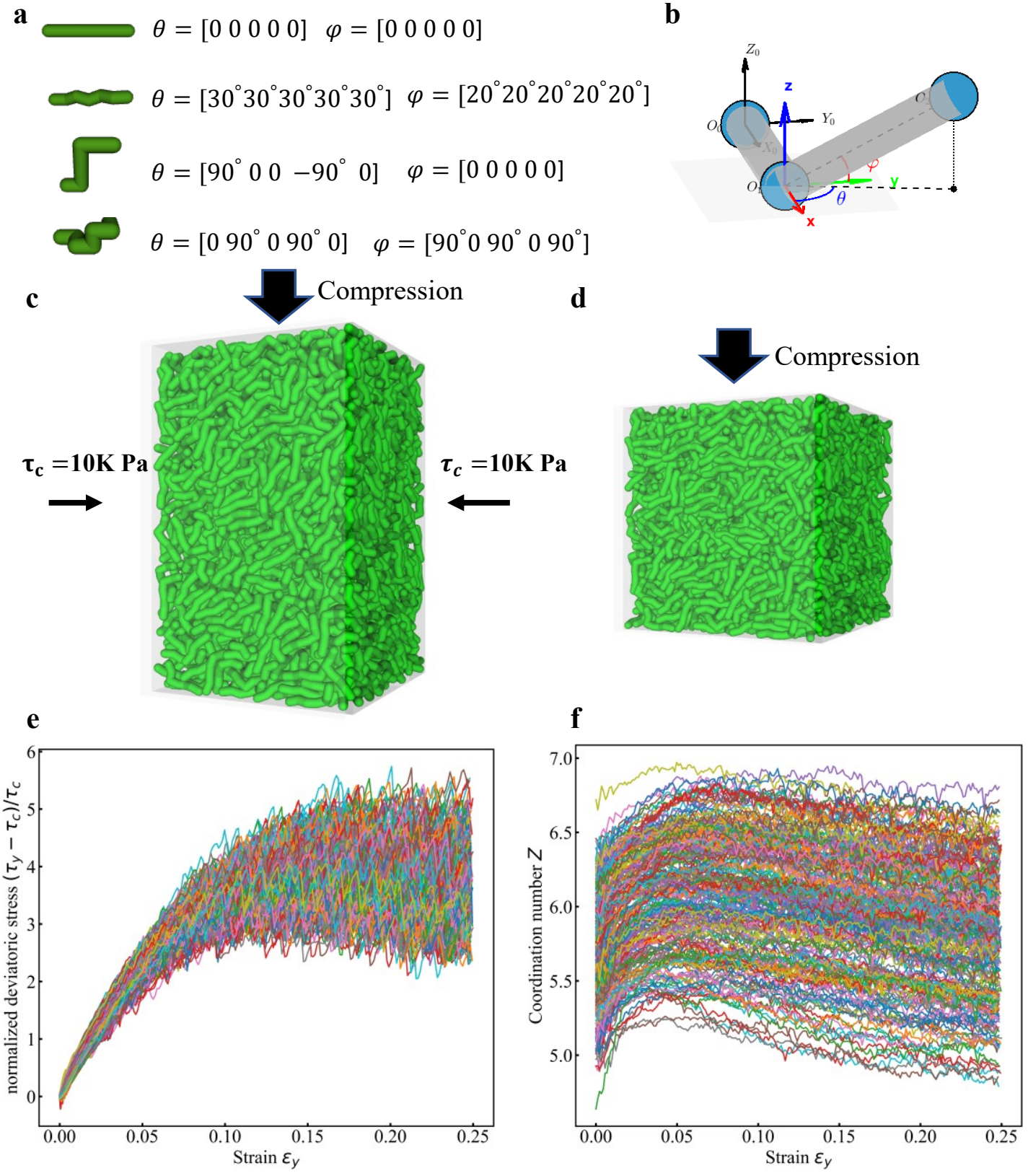

Figure 1: Particle geometry generation, DEM simulations, and shape-dependent mechanical response of entangled granular metamaterials. a) Representative particle geometries and their corresponding angle sequences (θ_i, φ_i), illustrating the transition from a baseline linear rod (AR=7) to complex, non-convex geometries. b) Schematic of the recursive geometric generation scheme using a local orthonormal coordinate system. c,d) Snapshots of the high-fidelity DEM simulations, depicting the granular assembly in its c) initial deposited state and d) final compressed state under triaxial loading. e) Macroscopic stress–strain curves for the initial dataset comprising 240 distinct geometries, exhibiting profound shape-induced heterogeneity in yield strength and hardening behavior. f) Evolution of the microscopic coordination number (Z) as a function of axial strain for the corresponding particle geometries.

Despite identical material properties and boundary conditions, the resulting stress–strain responses exhibit pronounced shape-induced heterogeneity as shown in Figure 1e. Such varying levels of mechanical response demonstrate that the efficacy of mechanical interlocking is fundamentally sensitive to the specific particle topology. Concurrently, the coordination number Z representing the average contact count per particle evolves distinctly across morphologies and serves as a microscopic descriptor of the contact network integrity presented in Figure 1f.

A statistical evaluation of the initial dataset reveals that while the vast majority of particle morphologies are densely clustered around a mean yield strength of 4.39, configurations approaching the observed maximum value of 5.74 are exceedingly rare (**Figure S2**, Supporting Information). This pronounced sparsity in the high-performance regime provides a rigorous empirical justification for adopting an uncertainty-aware active learning strategy, as a conventional random search would be overwhelmingly biased toward the high-density regions of moderate performance. The proposed framework is therefore explicitly designed to escape these dense basins and to extrapolate toward the elusive long tail of the distribution, where the rare geometric motifs responsible for superior load-bearing capacity reside.

2.2 Emergent Structure–Property Relationships within the Latent Morphological Space

Transforming the fragmented and high-dimensional configuration space into a searchable design domain is achieved through a Semi-Supervised Graph Wasserstein Autoencoder (SS-GWAE). This framework is specifically designed to overcome the severe data inefficiency inherent to deep generative models[32,33] within the context of granular mechanics where high-fidelity DEM labels are computationally prohibitive. We address this challenge via a semi-supervised paradigm[34] that exploits the pronounced asymmetry between the virtually unbounded geometric configuration space and the extremely limited availability of mechanical labels. While the geometric configuration space is virtually inexhaustible and allows for the rapid curation of 80,000 unlabeled particle shapes, the corresponding mechanical labels are restricted to a critically small-sample regime of only 240 DEM simulations.

The SS-GWAE architecture employs a dual-stream information flow that integrates geometric representation learning with sparse physical supervision. Particle morphologies are encoded as geometric graphs[35] where nodes represent spherical joints and edges correspond to rigid bonds to enable a natural description of articulated non-convex topologies independent of spatial orientation. Graph convolutional networks[36] are employed within the encoder to extract multi-scale geometric features and compress them into a 16-dimensional latent representation denoted as $\mathbf{z}$. To ensure kinematic validity, the decoder reconstructs the sequence of unit tangent vectors rather than absolute coordinates thereby preserving the physical bond length l_b across the entire generated library. Detailed architectural specifications and implementation strategies are provided in Section S2 of the Supporting Information.

Model training is governed by a composite objective function that jointly enforces geometric accuracy, latent-space regularity, and mechanical consistency,

$$\mathcal{L} = \mathcal{L}_{\text{recon}} + \lambda_{MMD}\mathcal{L}_{MMD} + \lambda_{\text{prop}}\mathcal{L}_{\text{prop}} \tag{4}$$

where the reconstruction loss $\mathcal{L}_{\text{recon}}$ minimizes angular deviations between predicted and ground-truth tangent vectors ensuring faithful geometric recovery. The Maximum Mean Discrepancy (MMD)[32] term $\mathcal{L}_{MMD}$ which is weighed by λ_{MMD} regularizes the latent distribution to promote smoothness and continuity. This characteristic is essential for stable interpolation and gradient-based exploration. The property loss $\mathcal{L}_{\text{prop}}$ which is scaled by λ_{prop} weakly anchors the latent coordinates to the macroscopic yield strength thereby imprinting sparse mechanical information onto the geometric manifold and transforming it into a physics-informed performance landscape. This synergistic formulation enables the model to capture complex morphological–mechanical relationships despite extreme label scarcity.

The reliability of the learned latent representation is first evaluated in terms of geometric reconstruction

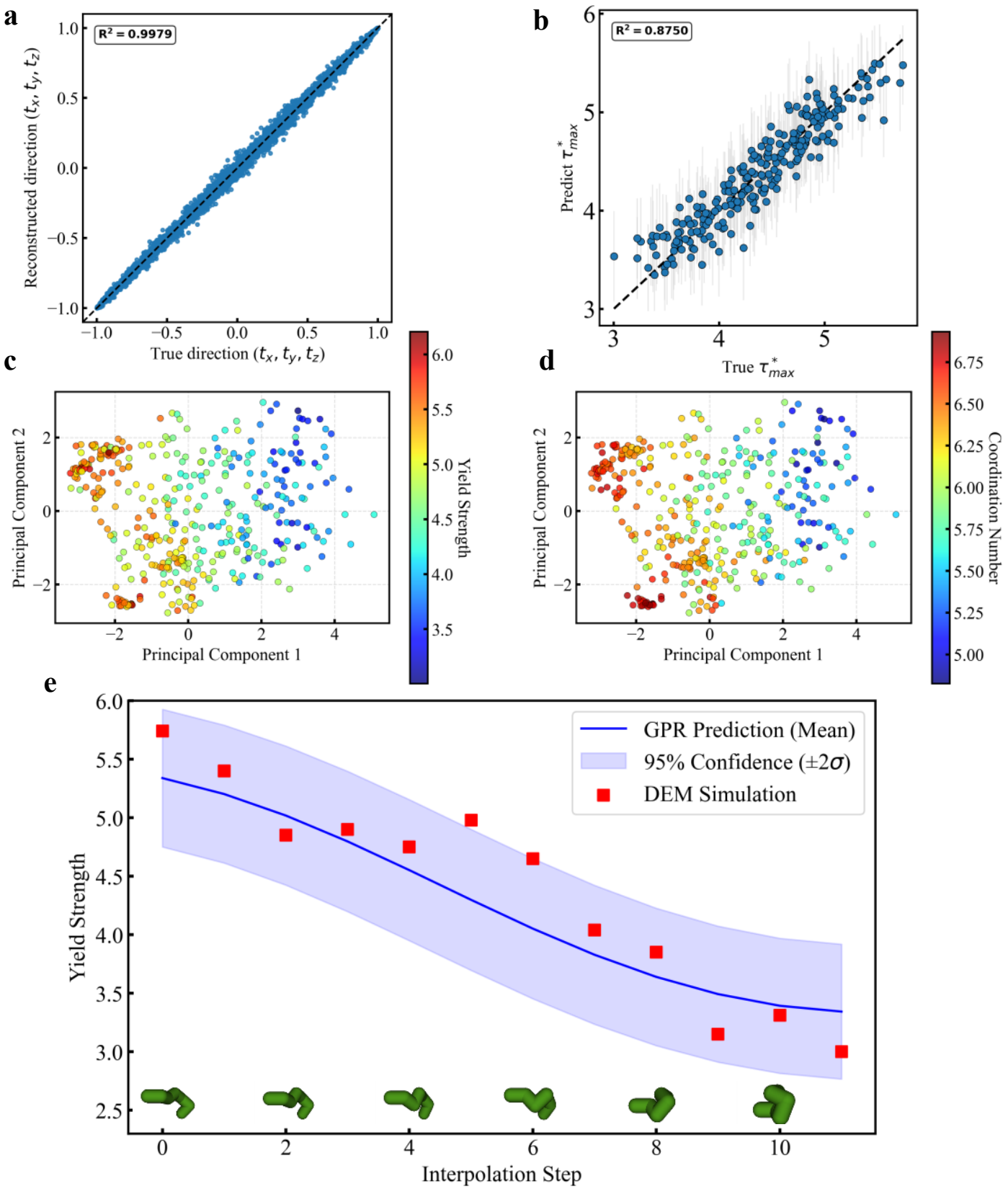

Figure 2: Representation fidelity and structural organization of the morphological manifold. a) Geometric reconstruction fidelity comparing predicted and ground-truth tangent vectors for the test set. b) GPR regression accuracy for yield strength evaluated via leave-one-out cross-validation. c, d) Latent manifold projected onto a PCA plane colored by c) yield strength and d) coordination number at peak stress. e) Manifold continuity verification through spherical linear interpolation illustrating the transition from expanded high-strength shape to a contracted low-strength shape.

accuracy and physical predictability. For an unseen test set of 2,000 samples, the reconstructed tangent vectors achieve a coefficient of determination of $R^2 = 0.999$ which indicates that the SS-GWAE accurately captures the essential morphological features of the particle geometries as shown in **Figure 2a**. To map latent representations to mechanical performance, Gaussian Process Regression (GPR) is employed as a probabilistic surrogate that accounts for the stochastic variability inherent in random granular packings.[37] The yield strength τ^*_{max} is modeled as a Gaussian random variable with a mean μ and a variance σ^2 according to the predictive distribution

$$f(\mathbf{z}) \sim \mathcal{N}(\mu(\mathbf{W}^\top \mathbf{z}), \sigma^2(\mathbf{W}^\top \mathbf{z})) \tag{5}$$

where the projection matrix $\mathbf{W}$[38] defines a compact physics-informed subspace that maximizes the correlation between latent geometry and strength. The surrogate model achieves a global R^2 of 0.875 under Leave-One-Out Cross-Validation (LOOCV)[39] which confirms that the latent manifold effectively captures the non-linear relationship between microscopic topology and macroscopic yield strength (Figure 2b).

Beyond predictive accuracy, the learned latent space exhibits an emergent structural organization that reflects the mechanics of geometric entanglement. A two-dimensional PCA projection reveals a clear performance gradient in which particle geometries are systematically arranged according to their interlocking efficacy (Figure 2c). Within this latent landscape, high-performance geometries occupy distinct functional regions on the left side of the manifold while the yield strength progressively decreases toward the right. Notably, the spatial distribution of the coordination number Z evaluated at the critical strain corresponding to peak strength closely mirrors this macroscopic performance organization as visualized in Figure 2d. This strong correspondence indicates that the latent representation implicitly encodes topological features associated with the formation of dense and mechanically resilient contact networks at failure. Importantly, this structure emerges without imposing explicit physical constraints during training which demonstrates that the framework autonomously captures the coupling between discrete particle topology and collective mechanical response.

Ensuring smoothness of the latent manifold with respect to physical properties is a prerequisite for effective gradient-informed shape optimization. Although such continuity is often assumed in generative modeling, its explicit validation is essential for granular systems where discrete contact dynamics can induce abrupt performance variations. To assess the navigability of the learned landscape, we select the best- and worst-performing particle shape in the initial dataset and construct a transition path via spherical linear interpolation.[18] As shown in Figure 2e, particle morphologies evolve smoothly from spatially extended to compact configurations without topological discontinuities. This progressive contraction correlates with a monotonic reduction in yield strength as rod-like geometries promote enhanced geometric interference and interlocking, whereas compact near-spherical shapes provide diminished resistance to macroscopic shear.

Consistent with this observation, yield strengths evaluated by high-fidelity DEM simulations exhibit a monotonic decline that closely follows the GPR predictions across the entire performance range. This agreement confirms that the latent manifold is both continuous and physically well-behaved thereby providing a reliable foundation for subsequent design optimization. However, this interpolation remains restricted to regions of the latent space supported by the training data which motivates the need for controlled morphological extrapolation to identify novel particle geometries that can achieve unprecedented mechanical performance beyond the limits of the random ensemble.

2.3 Uncertainty-Aware Active Learning and Autonomous Discovery

To efficiently explore the high-dimensional latent design space under strict computational constraints, we implement a closed-loop uncertainty-aware active learning framework[29] that integrates database generation, probabilistic surrogate modeling, stochastic optimization, and DEM validation as illustrated in

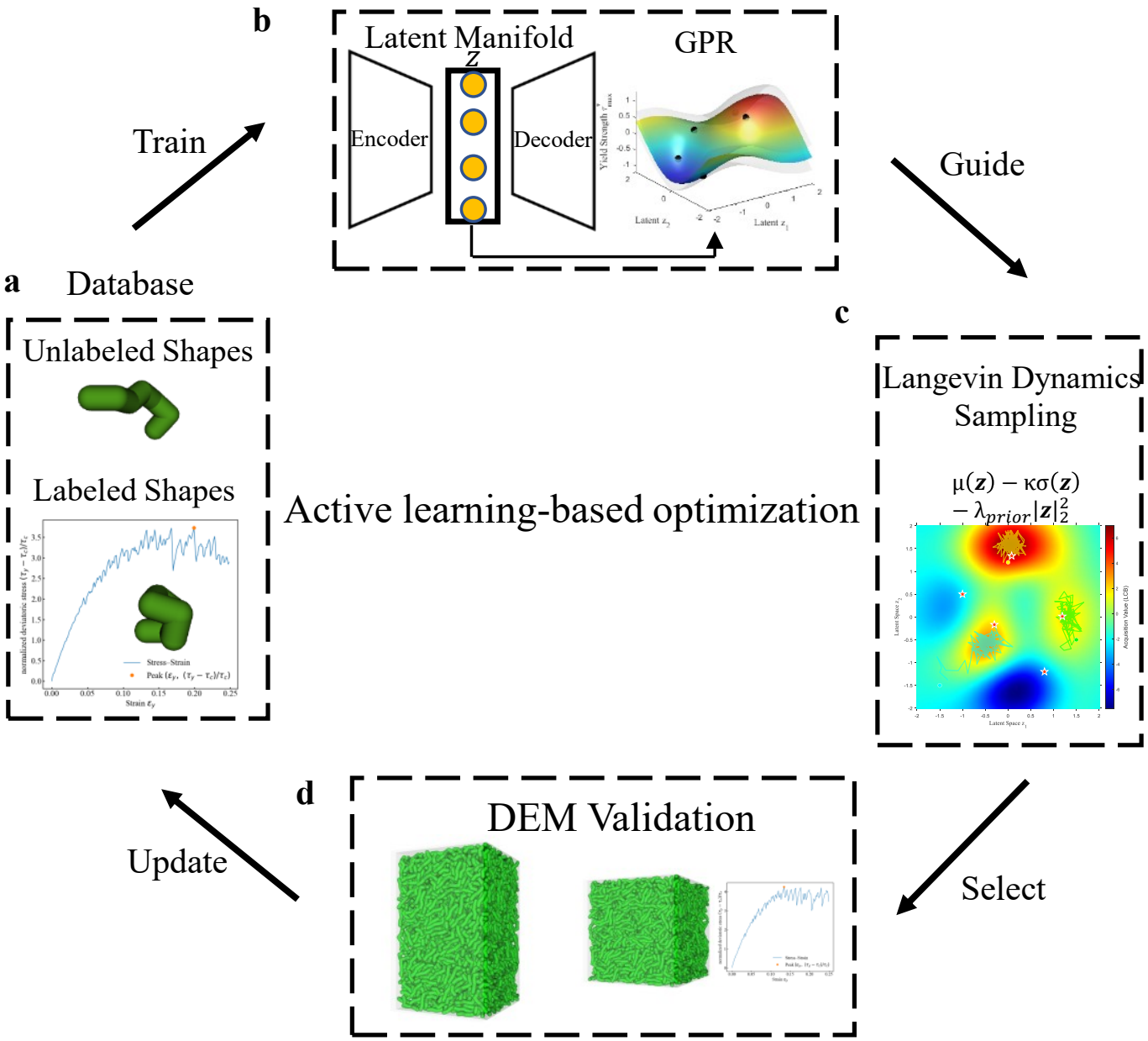

Figure 3: Active learning framework for the autonomous discovery of high-performance particle geometries. a) Database architecture integrating unlabeled shapes and labeled simulations. b) Probabilistic surrogate modeling using Gaussian Process Regression within the latent manifold. c) Stochastic optimization via Langevin dynamics sampling guided by the acquisition function. d) High-fidelity DEM validation providing iterative feedback to close the design loop.

Figure 3. This discovery paradigm enables targeted geometric extrapolation beyond data-supported regions while maintaining physical reliability throughout the iterative process.

At each iteration, a Gaussian Process Regression (GPR) surrogate is trained on the accumulated set of labeled high-fidelity DEM simulations as shown in **Figure 3a, b** while the broader pool of unlabeled geometries is leveraged to maintain a well-structured latent manifold. The surrogate maps latent coordinates to a probabilistic performance landscape providing both the expected yield strength $\mu(\mathbf{z})$ and an explicit estimate of epistemic uncertainty $\sigma(\mathbf{z})$ which represents an essential capability in a regime where simulation data are scarce and costly. To balance exploitation, exploration, and physical admissibility, we define a conservative acquisition function $\mathcal{A}(\mathbf{z})$ as expressed

$$\mathcal{A}(\mathbf{z}) = \mu(\mathbf{z}) - \kappa \cdot \sigma(\mathbf{z}) - \lambda_{prior}\|\mathbf{z}\|_2^2 \tag{6}$$

In this formulation, $\mu(\mathbf{z})$ promotes regions of high expected yield strength while the uncertainty penalty $\kappa \cdot \sigma(\mathbf{z})$ suppresses unreliable extrapolations and the quadratic prior regularization $\lambda_{prior}\|\mathbf{z}\|_2^2$ confines the search to the physically admissible latent manifold. This synergistic approach prevents the optimizer from exploiting spurious high-mean predictions unsupported by data.

To ensure a comprehensive exploration of this complex landscape and prevent premature convergence to redundant local optima, we further implement a clustering-based seeding strategy. Specifically, an elite subset comprising the top 10% of samples ranked by yield strength is identified and partitioned into K distinct clusters via K-means in the latent space. The highest-performing sample from each cluster serves as an initialization seed which enables the launch of parallel optimization trajectories from distinct basins of attraction as illustrated in (**Figure S4**). Optimization of the acquisition landscape is performed using Stochastic Gradient Langevin Dynamics (SGLD)[40] which interprets the search as the stochastic evolution of a particle in an effective potential field $\mathcal{A}(\mathbf{z})$. The latent state evolves according to the discretized Langevin update

$$\mathbf{z}_{t+1} = \mathbf{z}_t + \eta\nabla_{\mathbf{z}}\mathcal{A}(\mathbf{z}) + \sqrt{2\eta}\cdot\boldsymbol{\epsilon}_t, \quad \boldsymbol{\epsilon}_t \sim \mathcal{N}(0, \mathbf{I}) \tag{7}$$

Here, $\mathbf{z}_t$ denotes the latent representation at iteration t and the injected Gaussian noise $\boldsymbol{\epsilon}_t$ provides thermal-like fluctuations that enable escape from shallow local optima and traversal of energy barriers. This stochasticity is critical for systematically probing the sparsely sampled and high-performance tails of the design distribution. Following Langevin-guided exploration, a diversity-driven selection strategy based on Farthest Point Sampling[41] identifies a batch of geometrically distinct candidates. These candidates are subsequently validated via high-fidelity DEM simulations as shown in Figure 3c, d and the resulting ground-truth yield strengths are assimilated into the training set to refine the surrogate model.

The closed-loop optimization was conducted over 10 iterations with a batch size of 12 resulting in a total of 120 new high-fidelity DEM evaluations. The efficiency of the search is reflected in the convergence history which exhibits a punctuated and stepwise improvement in mechanical performance as illustrated in **Figure 4a**. Owing to the sparse and noisy mapping between latent geometry and macroscopic yield strength, local surrogate gradients do not necessarily provide reliable ascent directions and may correspond to spurious performance peaks. In this context the uncertainty-aware sampling strategy effectively suppresses unreliable regions of the design space and enables robust exploration. As a result the framework identifies particle geometries achieving a peak yield strength of 6.21 which represents a substantial improvement over the maximum value of 5.74 observed in the initial random ensemble.

Beyond isolated extrema the population-level statistics reveal a systematic rightward shift in performance. As shown in Figure 4b the mean yield strength of the optimized population increases from 4.39 to 4.76 indicating a global enhancement of mechanical robustness. Notably the rare high-performance tail that characterized the initial random distribution effectively becomes the new baseline after optimization which highlights the framework's ability to promote exceptional geometries from statistical outliers to representative solutions.

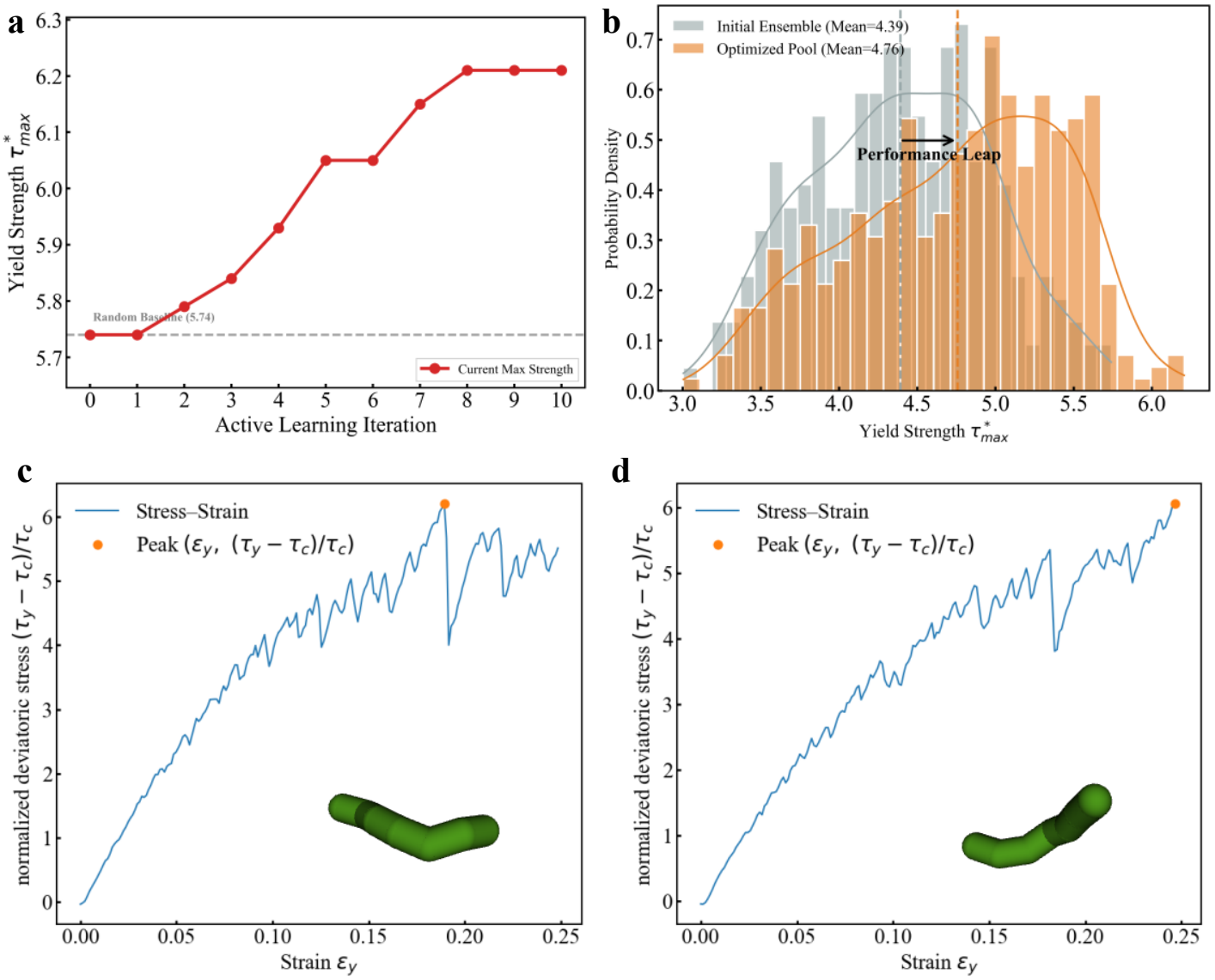

Figure 4: Quantitative performance evolution and identification of non-unique optimal morphologies. a) Convergence history of the maximum yield strength throughout the iterative active learning process where the punctuated ascent highlights the framework's capability to navigate toward high-performance regimes. b) Statistical distribution of yield strength for the final optimized pool compared to the initial random ensemble illustrating a systemic rightward shift toward superior interlocking performance. c, d) Mechanical response signatures and three-dimensional architectures for c) Type A which exhibits rapid shear resistance mobilization and d) Type B which demonstrates sustained strain-hardening and a delayed peak response.

A key outcome of this diversity-aware search is the emergence of non-unique optimal solutions manifested as two distinct particle shapes denoted as Type A and Type B. While both shapes attain comparable peak yield strengths they exhibit qualitatively different mechanical signatures in their stress-strain responses as shown in Figure 4c, d. Type A displays a rapid mobilization of shear resistance reaching its peak at a relatively small axial strain of approximately 0.18. In contrast Type B follows a more gradual hardening trajectory where peak stress is delayed until an axial strain of about 0.25. Despite these differences both responses exhibit pronounced strain-hardening behavior prior to failure.

This divergence indicates that extreme yield strength can be achieved through multiple and mechanically distinct force-network architectures induced by different particle morphologies. The coexistence of these optimal yet disparate solutions underscores the ability of the proposed framework to uncover the rich morphological diversity underpinning superior topological interlocking.

2.4 Experimental Validation of Geometry-Induced Mechanical Performance

To bridge the gap between computational discovery and physical reality, we conducted mechanical experiments using a bespoke confined compression apparatus designed for the stable characterization of entangled granular assemblies as illustrated in **Figure 5a**. The experimental setup features a rectangular chamber with fixed anterior and posterior walls while incorporating movable side walls that are specifically engineered to mitigate tilting moments and ensure uniform load distribution. We evaluated three representative geometries where light blue denotes the rod benchmark and green signifies the highest-performing random sample while orange represents the optimized Type A geometry to verify the performance hierarchy predicted by our virtual design framework. This color convention is maintained consistently across all experimental visualizations and quantitative plots to ensure visual clarity.

Force–displacement responses were obtained by averaging five independent compression trials for each morphology where solid curves denote the mean response and shaded bands indicate the standard deviation as shown in Figure 5b. The results reveal a clear mechanical progression in which the optimized geometry significantly outperforms both the rod baseline and the random optimum. Specifically, the orange curves exhibit a notably stiffer response and achieve a substantially higher peak force which confirms that the morphological features identified by our framework successfully translate into superior load-bearing capacity in physical implementations. The close agreement between experimental measurements and corresponding numerical predictions represented by dashed curves confirms the fidelity of the digital twin framework and demonstrates that the performance enhancement arises from the designed geometric features rather than stochastic packing effects.

The physical origin of this enhanced performance is further elucidated through the visual assessment of kinematic evolution under compression as depicted in Figure 5c–e. While granular assemblies typically accommodate vertical loading through lateral dilation driven by particle sliding and rotation, the optimized Type A assembly exhibits a pronounced suppression of lateral expansion. As highlighted by the red boxes in Figure 5e, the expanded and non-convex limbs of the optimized particles induce strong geometric entanglement that effectively pins the contact network. This self-locking mechanism imposes topological constraints that inhibit relative particle motion which directly suppresses macroscopic volume expansion and transforms the granular bed into a coherent load-bearing structure stabilized purely by geometry.

Finally, we conclude the mechanical characterization by evaluating the potential of geometric complexity to overcome conventional aspect-ratio limitations for self-supporting granular structures by measuring the angle of repose following the gravity-driven collapse of a cylindrical column comprising 1,000 particles. Representative final configurations obtained from numerical simulations and physical experiments are depicted in **Figure 6a–c**. The rod-shaped particles display fluid-like behavior with a low angle of repose of 18.2° whereas the best random design increases this stability to 33.5°. Strikingly the optimized geometry forms a steep and mechanically stable pile with an angle of repose of 41.9°. This

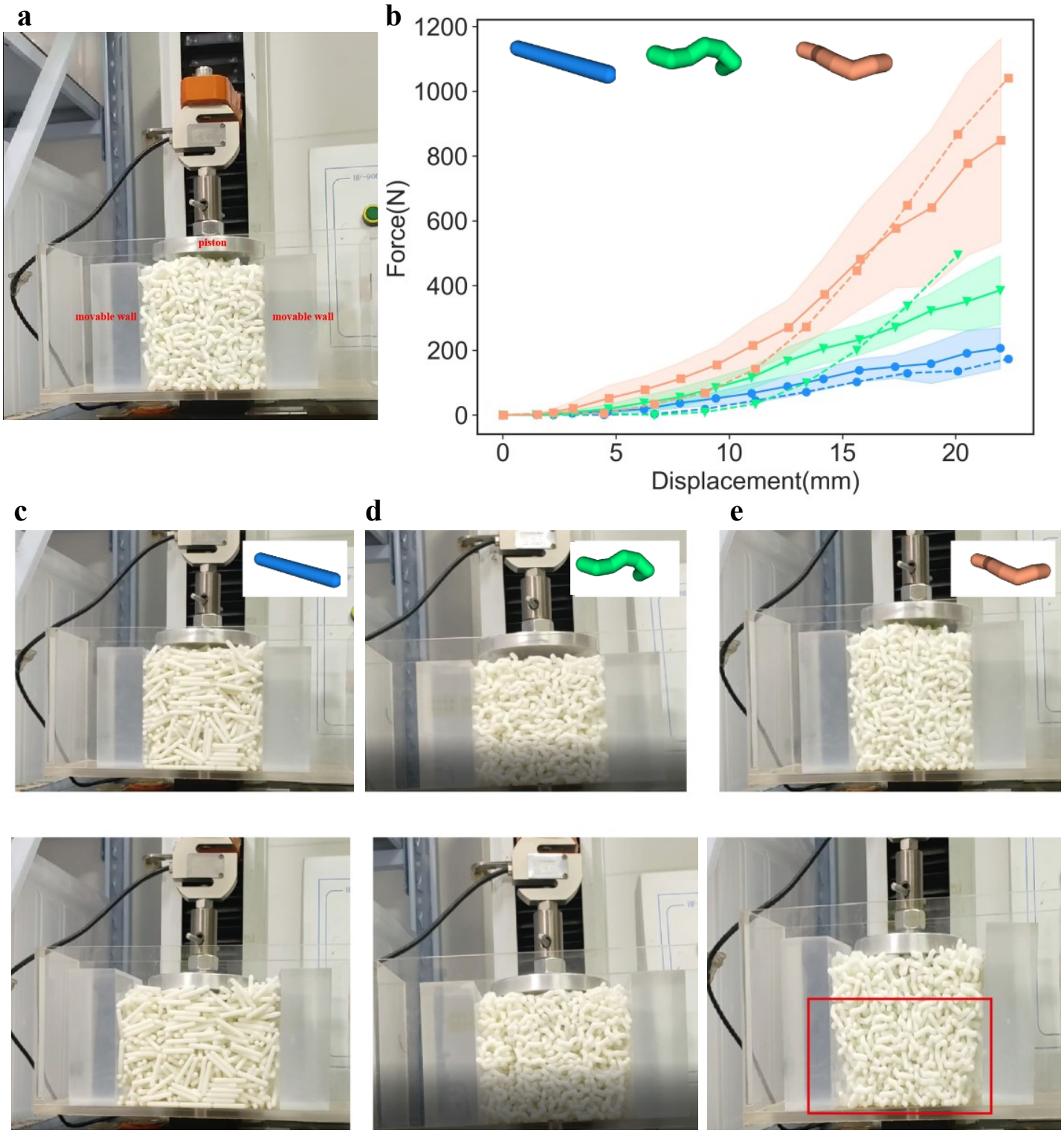

Figure 5: Experimental validation of the performance hierarchy. a) Photographic view and schematic illustration of the bespoke confined compression rig engineered for stable macroscopic characterization. b) Force–displacement profiles comparing experimental measurements where solid lines signify the mean of five independent trials with shaded regions representing the standard deviation and dashed lines indicate the corresponding numerical simulations. c, d, e) Experimental visualization of the kinematic evolution from the initial to compressed states for c) the rod benchmark, d) the best random sample, and e) the optimized geometry where red boxes highlight the suppressed lateral dilation facilitated by the self-locking effect.

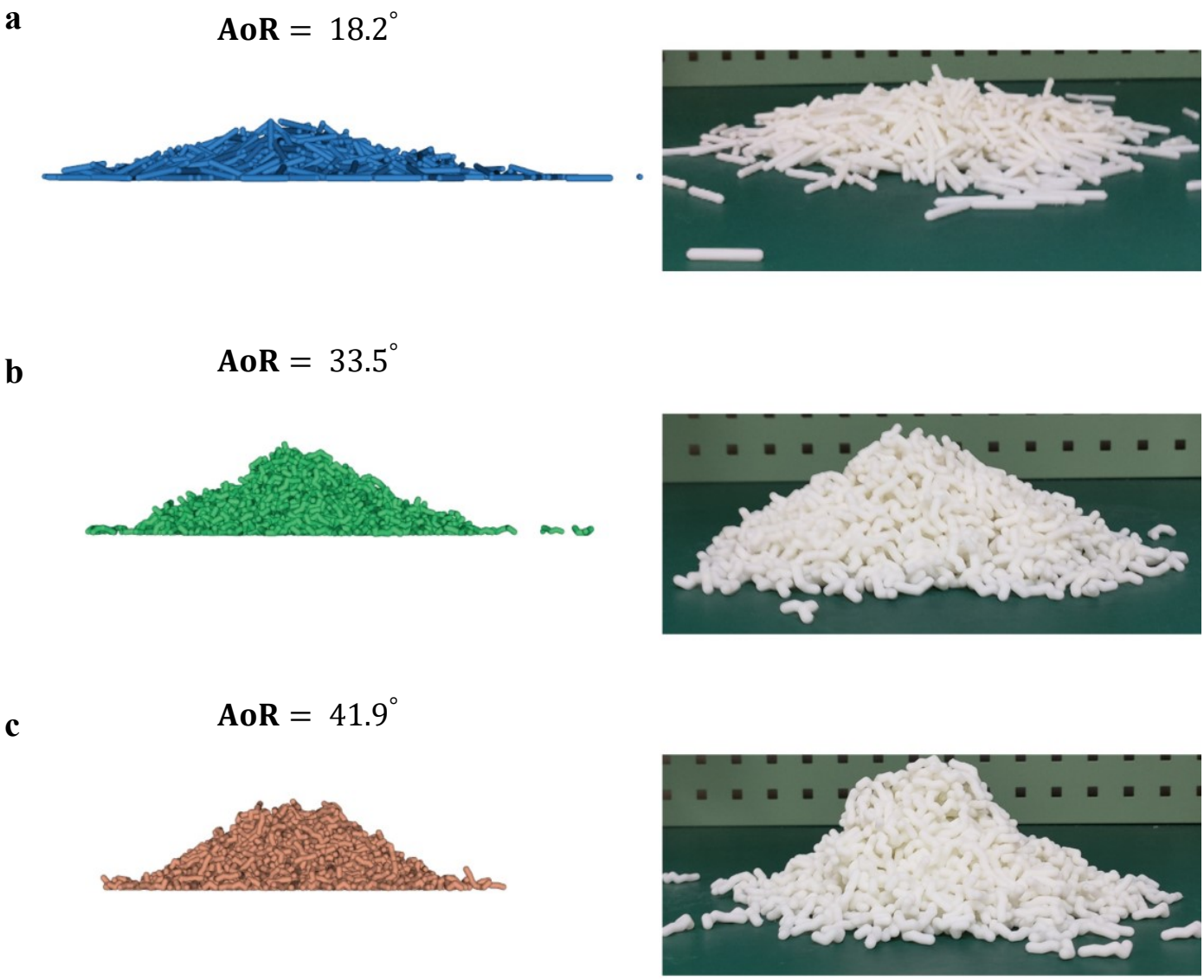

Figure 6: Evaluation of emergent self-supporting capability via Angle of Repose (AoR) tests. Comparison of the final resting structures for (a) the rod benchmark, (b) the best random sample, and (c) the optimized shape.

substantial enhancement demonstrates that the engineered topological entanglement successfully imparts quasi-cohesive behavior to the assembly. Such self-supporting characteristics are typically associated with high-aspect-ratio fibers[30] yet are achieved here through autonomous shape optimization in comparatively low-aspect-ratio particles.

3 Conclusion

In summary, this work establishes a data-efficient and uncertainty-aware design paradigm for entangled granular materials, enabling the autonomous discovery of particle geometries that significantly enhance macroscopic mechanical performance under strict computational constraints. By integrating semi-supervised geometric representation learning with stochastic, uncertainty-penalized optimization, the proposed framework overcomes the long-standing limitations imposed by the high dimensionality of non-convex shape spaces and the prohibitive cost of DEM simulations.

Beyond algorithmic advancement, the optimized geometries reveal a clear physical mechanism underlying their superior performance. The transition from friction-dominated resistance to cooperative geometric interlocking suppresses shear localization and lateral dilatancy, effectively transforming a disordered granular assembly into a coherent load-bearing architecture. Importantly, this behavior is achieved in particles with comparatively low aspect ratios, demonstrating that non-convexity and topological complexity—rather than slenderness alone—govern macroscopic strength and self-supporting capability in entangled granular media.

Experimental validation using additively manufactured particles confirms the predicted mechanical hierarchy and verifies the high fidelity of the numerical framework. The emergence of stable, self-supporting piles with large angles of repose provides direct physical evidence that geometry-driven entanglement can impart quasi-cohesive behavior to granular systems without altering material properties.

More broadly, the proposed framework is not limited to entangled granular materials. Its ability to operate reliably in data-scarce, stochastic, and non-differentiable design landscapes suggests broad applicability to other classes of architected and disordered materials. This work therefore opens a pathway toward scalable, physics-guided autonomous discovery in complex material systems where traditional trial-and-error design is infeasible.

Supporting Information

Supporting Information is available from the Wiley Online Library or from the author.

Acknowledgements

This work was financially supported by the Zhejiang Provincial Natural Science Foundation of China (NO. LZ24A020002), National Natural Science Foundation of China (NOs. 12372250 and 12132015), and Specialized Research Projects of Huanjiang Laboratory (NO. XYY-128102-E52201).

References

[1] D. Haver, D. Acuña, S. Janbaz, E. Lerner, G. Düring, C. Coulais, *Proceedings of the National Academy of Sciences* **2024**, *121*, 11.

[2] A. Rezanejad, M. Mousa, C. D. Lorenz, M. Howard, A. E. Forte, *Advanced Functional Materials* **2025**, *35*.

[3] Z. Meng, H. Yan, Y. Wang, *Science Advances* **2024**, *10*, 36.

[4] P. Wang, T. Pähtz, K. Luo, Y. Guo, *Physical Review E* **2025**, *111*.

[5] K. Fu, Z. Zhao, L. Jin, *Advanced Functional Materials* **2019**, *29*, 32.

[6] Y. Guo, J. S. Curtis, *Annual Review of Fluid Mechanics* **2015**, *47* 21.

[7] J. Zhao, S. Zhao, S. Luding, *Nature Reviews Physics* **2023**, *5* 505.

[8] N. Gravish, S. V. Franklin, D. L. Hu, D. I. Goldman, *Physical Review Letters* **2012**, *108*, 20.

[9] K. A. Murphy, N. Reiser, D. Choksy, C. E. Singer, H. M. Jaeger, *Granular Matter* **2016**, *18*, 1.

[10] K. Karapiperis, S. Monfared, R. B. de Macedo, S. Richardson, J. E. Andrade, *Granular Matter* **2022**, *24*, 4.

[11] D. P. Huet, M. Jalaal, R. van Beek, D. van der Meer, A. Wachs, *Physical Review Fluids* **2021**, *6*, 10.

[12] Y. Zhao, K. Liu, M. Zheng, J. Barés, K. Dierichs, A. Menges, R. P. Behringer, *Granular Matter* **2016**, *18*, 1.

[13] Y. Zhao, J. Barés, J. E. S. Socolar, *Physical Review E* **2020**, *101*, 6.

[14] J. Landauer, M. Kuhn, D. S. Nasato, P. Foerst, H. Briesen, *Powder Technology* **2020**, *361* 711.

[15] M. Z. Miskin, H. M. Jaeger, *Nature Materials* **2013**, *12* 326.

[16] J. Qin, G. S. Khaira, Y. Su, G. P. Garner, M. Miskin, H. M. Jaeger, J. J. de Pablo, *Soft Matter* **2013**, *9* 11467.

[17] K. Karapiperis, J. E. Andrade, *Extreme Mechanics Letters* **2021**, *42* 101041.

[18] L. Zheng, K. Karapiperis, S. Kumar, D. M. Kochmann, *Nature Communications* **2023**, *14*, 1.

[19] J.-H. Bastek, S. Kumar, B. Telgen, R. N. Glaesener, D. M. Kochmann, *Proceedings of the National Academy of Sciences* **2021**, *119*, 1.

[20] M. A. Bessa, P. Glowacki, M. Houlder, *Advanced Materials* **2019**, *31*, 48.

[21] Z. Chafia, J. Yvonnet, J. Bleyer, *Computer Methods in Applied Mechanics and Engineering* **2025**, *437* 117747.

[22] Z. Xu, S. Zhang, X. Sun, S. Mao, R. Xiao, *Advanced Functional Materials* **2025**.

[23] P. T. Nguyen, Y. Heider, D. M. Kochmann, F. Aldakheel, *Computer Methods in Applied Mechanics and Engineering* **2026**, *449* 118499.

[24] J. Wang, W. Chen, D. Da, M. Fuge, R. Rai, *Computer Methods in Applied Mechanics and Engineering* **2022**, *396* 115060.

[25] Y. Zang, P.-S. Koutsourelakis, *Computer Methods in Applied Mechanics and Engineering* **2026**, *450* 118597.

[26] L. Lu, P. Jin, G. Pang, Z. Zhang, G. E. Karniadakis, *Nature Machine Intelligence* **2021**, *3* 218.

[27] M. Raissi, P. Perdikaris, G. E. Karniadakis, *Journal of Computational Physics* **2019**, *378* 686.

[28] M. Ostoja-Starzewski, *Journal of Applied Mechanics* **2001**, *69*, 1 25.

[29] T. Lookman, P. V. Balachandran, D. Xue, R. Yuan, *npj Computational Materials* **2019**, *5*, 1.

[30] Y. Jung, T. Plumb-Reyes, H.-Y. G. Lin, L. Mahadevan, *Proceedings of the National Academy of Sciences* **2025**, *122*.

[31] Y. Guo, Y. Li, Q. Liu, H. Jin, D. Xu, C. Wassgren, J. S. Curtis, *AIChE Journal* **2020**, *66*, 11.

[32] I. Tolstikhin, O. Bousquet, S. Gelly, B. Schoelkopf, *arXiv preprint arXiv:1711.01558* **2017**.

[33] B. Sanchez-Lengeling, A. Aspuru-Guzik, *Science* **2018**, *361*, 6400 360.

[34] D. P. Kingma, D. J. Rezende, S. Mohamed, M. Welling, In *Advances in Neural Information Processing Systems*, volume 27. **2014** .

[35] M. M. Bronstein, J. Bruna, T. Cohen, P. Veličković, *arXiv preprint arXiv:2104.13478* **2021**.

[36] T. N. Kipf, M. Welling, *arXiv preprint arXiv:1609.02907* **2016**.

[37] C. Williams, C. Rasmussen, In *Advances in Neural Information Processing Systems*, volume 8. **1995** .

[38] S. Wold, M. Sjöström, L. Eriksson, *Chemometrics and Intelligent Laboratory Systems* **2001**, *58*, 2 109.

[39] S. Arlot, A. Celisse, *Statistics Surveys* **2010**, *4* 40.

[40] M. Welling, Y. W. Teh, In *Proceedings of the 28th International Conference on Machine Learning (ICML-11)*. **2011** 681–688.

[41] Y. Eldar, M. Lindenbaum, M. Porat, Y. Y. Zeevi, *IEEE Transactions on Image Processing* **1997**, *6*, 9 1305.